Electronic Supplementary Material (ESI) for Nanoscale.

Supporting Information

Electrochromic-Supercapacitor Based on MOF Derived Hierarchical-Porous NiO Film

Shengyu Zhou[a#], Shen Wang[a#], Shijin Zhou[a], Hongbo Xu[a*], Jiupeng Zhao[a], Jing Wang[c], Yao Li[b*]

1 The preparation of FTO-Fe_2O_3

$FeCl_3 \cdot 6H_2O$(1 g), Na_2SO_4(1.2 g), and NH_4F(0.5 g) were dissolved into 50 ml de-ionized water, then the solution and FTO (tipsily placed) were transferred into reaction still with the temperature of 100 ℃ for 10 h. After the reactor returned to the room temperature, the sample was washed with de-ionized water and dried in the flowing nitrogen. Then, it was heated under Ar for 3 h at 550 ℃ with a heating rate of 2 ℃ min^{-1}.

2. Assembly of the device

We utilized the ITO-NiO-2 as the positive electrode, FTO-Fe_2O_3 as the negative electrode and 1 M KOH aqueous as the electrolyte. Firstly, the positive and negative electrode were separated by nano-tape, then UV curing adhesive was used for packaging the device (leaving a small gap to inject the electrolyte) with the lighting of a UV lamp. Second, the electrolyte was injected by the injector, and then the whole device was packaged by the UV curing adhesive.

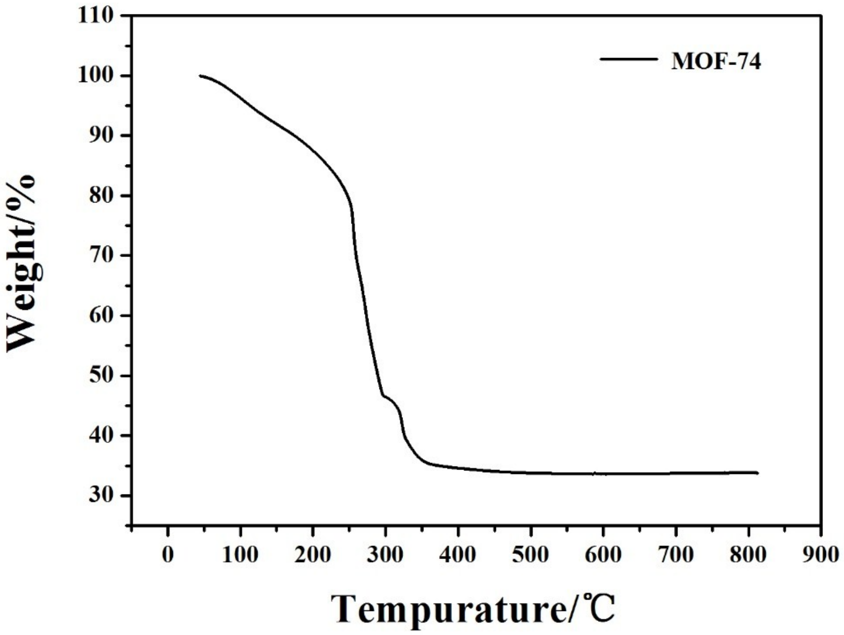

Figure S1. TGA traces of MOF-74 powder at the heating rate of 5 °C/min in a nitrogen atmosphere.

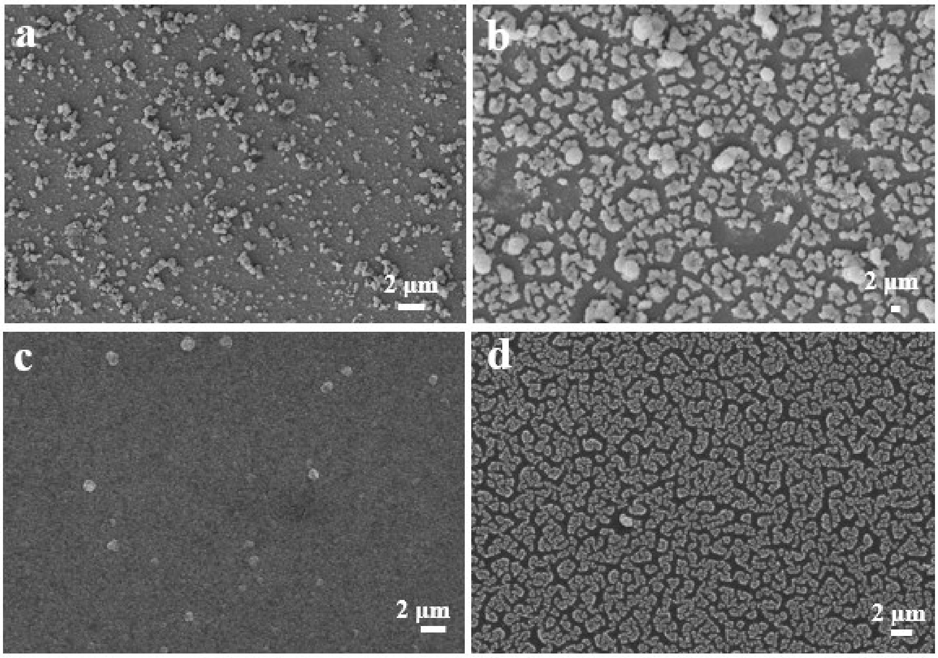

Figure S2. SEM imagines of MOF-74 film and NiO film on ITO: (a) ITO-MOF-1, (b) ITO-NiO-1, (c) ITO-MOF-3, and (d) ITO-NiO-3.

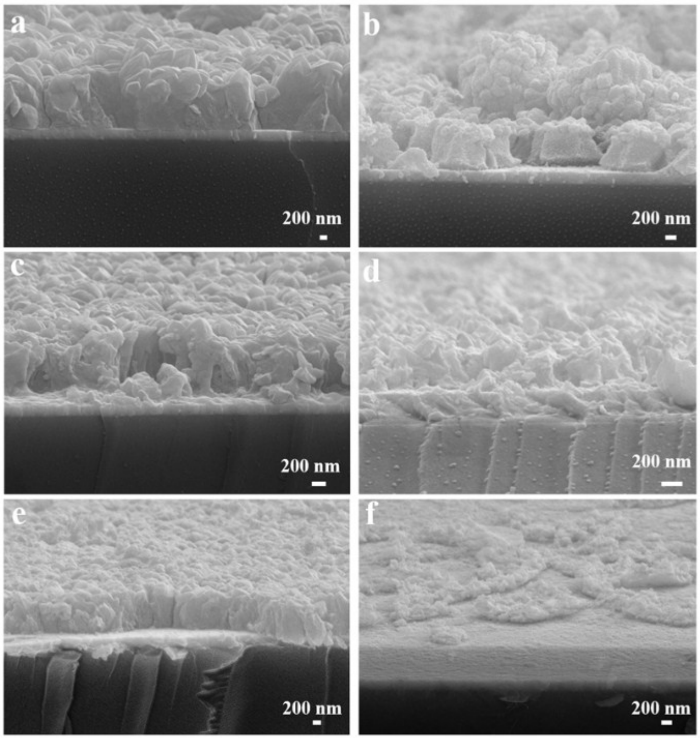

Figure S3. Cross-sectional SEM images of the MOF-74 film and NiO film: (a) ITO-MOF-1, (b) ITO-NiO-1, (c) ITO-MOF-2, (d) ITO-NiO-2, (e) ITO-MOF-3, and (f) ITO-NiO-3.

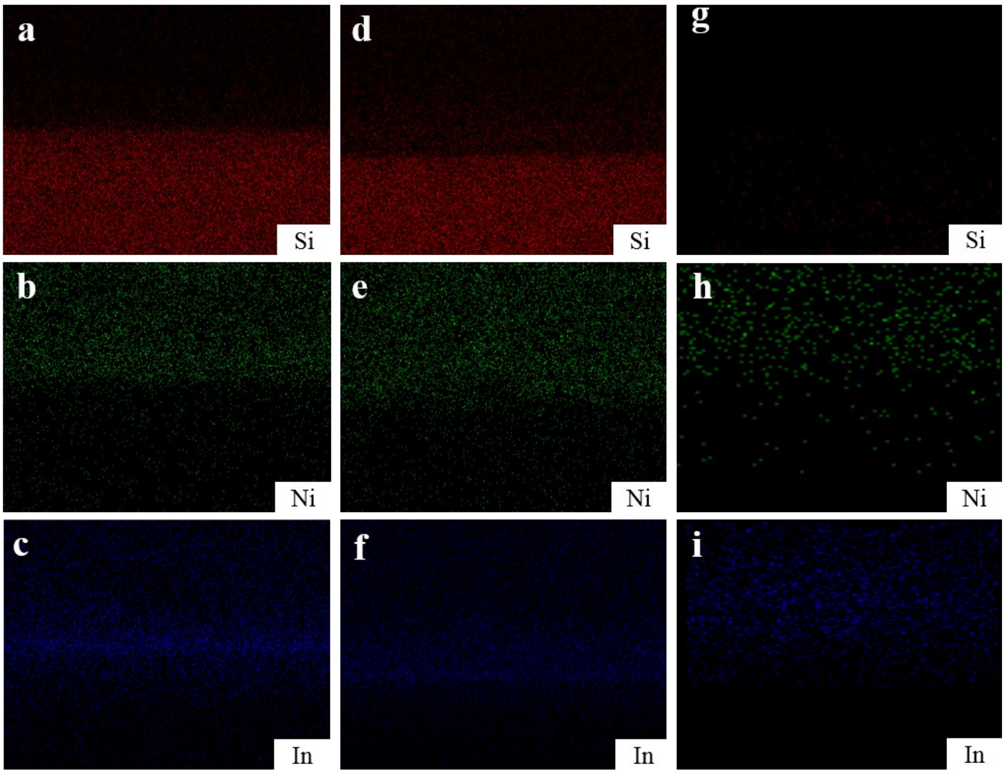

Figure S4. Element mapping of NiO film with different concentrations: (a, b, c) ITO-NiO-1, (d, e, f) ITO-NiO-2, and (g, h, i) ITO-NiO-3.

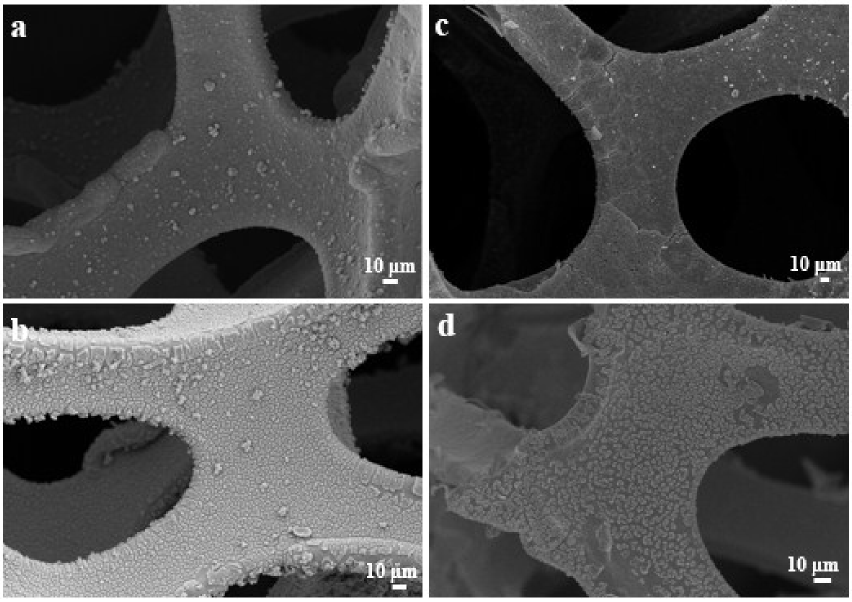

Figure S5. SEM imagines of MOF-74 film and NiO film on nickel foam: (a) NF-MOF-1, (b) NF-NiO-1, (c) NF-MOF-3, and (d) NF-NiO-3.

The larger particles are shown on NF-MOF-1 films and NF-NiO-1 films (Figure S5a and S5b). As the concentration decreases, the MOF-74 film is flat and the NiO particles are uniformly distributed on Ni foam after annealing. When the concentration is 9.37 mmol, some of the membranes fell off due to the relatively large internal shrinkage stresses on the film. But the NiO film with a concentration of 7.03 mmol is more uniformly distributed (the average size and spacing distance are about 300 nm and 200 nm, respectively) in Figure 1c and d. When the concentration is 5.62 mmol, the NF-MOF-3 film is flat and dense, but the NF-NiO-3 film presents a larger spacing distance and average size (Figure S5c and S5d). The average size and spacing of the NiO particles are about 1 μm and 2 μm, respectively. That is due to the thin thickness of the film and large volume contraction. According to the compare of SEM images between films on ITO and Ni foam, it can be seen that the morphology of MOF-74 film and NiO film on the Ni foam are basically the same as those on ITO. This result demonstrates that the choice of substrates has no influence on the morphologies of the films.

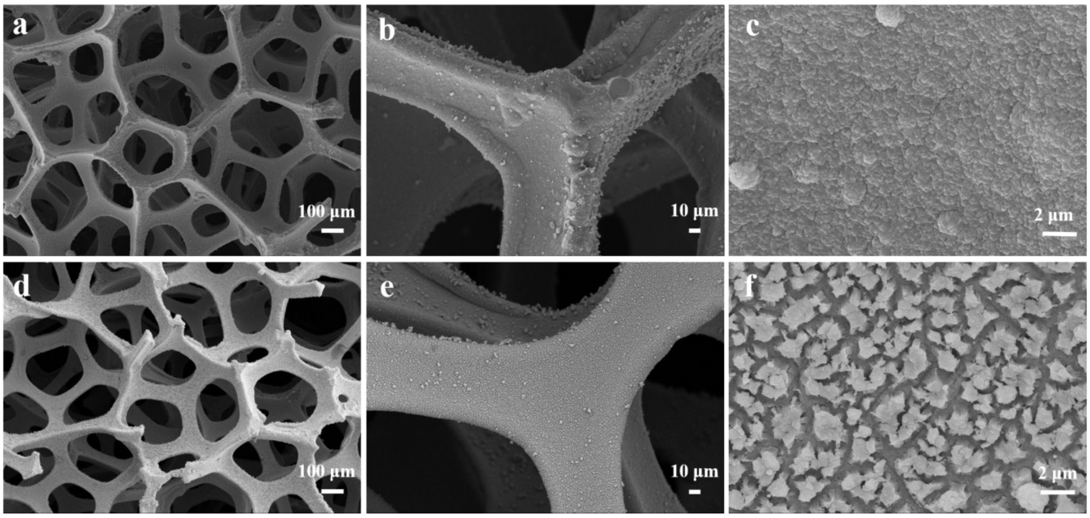

Figure S6. SEM imagines of MOF-74 film and NiO film on nickel foam: (a, b, c) NF-MOF-2, and (d, e, f) NF-NiO-2.

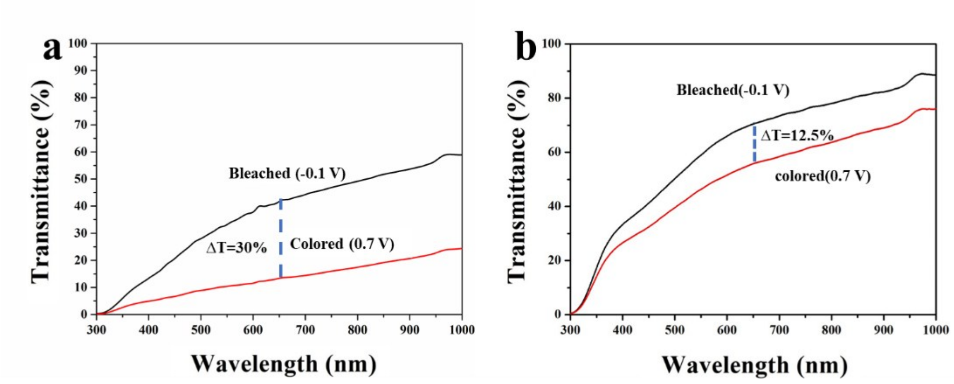

Figure S7. Transmission spectra of different NiO films on ITO: (a) ITO-NiO-1, and (b) ITO-NiO-3.

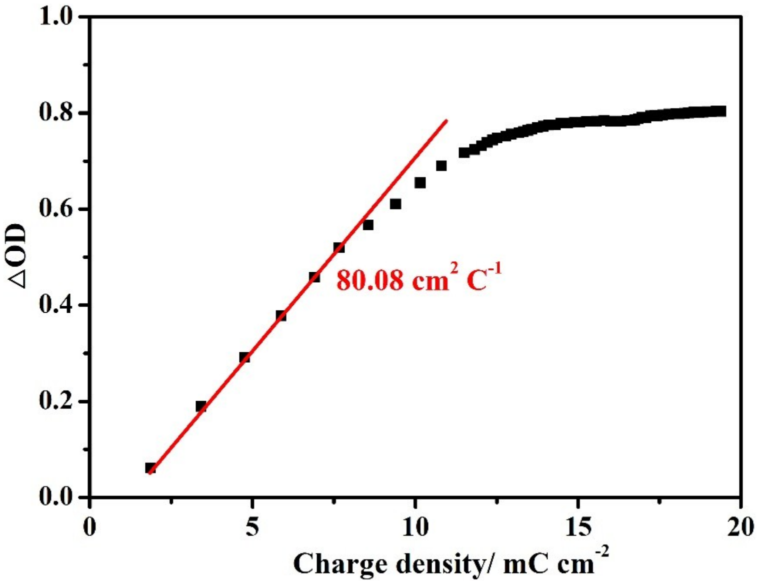

Figure S8 Variation of the in situ optical density. (△OD vs. the deintercalated charge density (Q) for the ITO-NiO-2 in 1 M KOH solution at 650 nm)

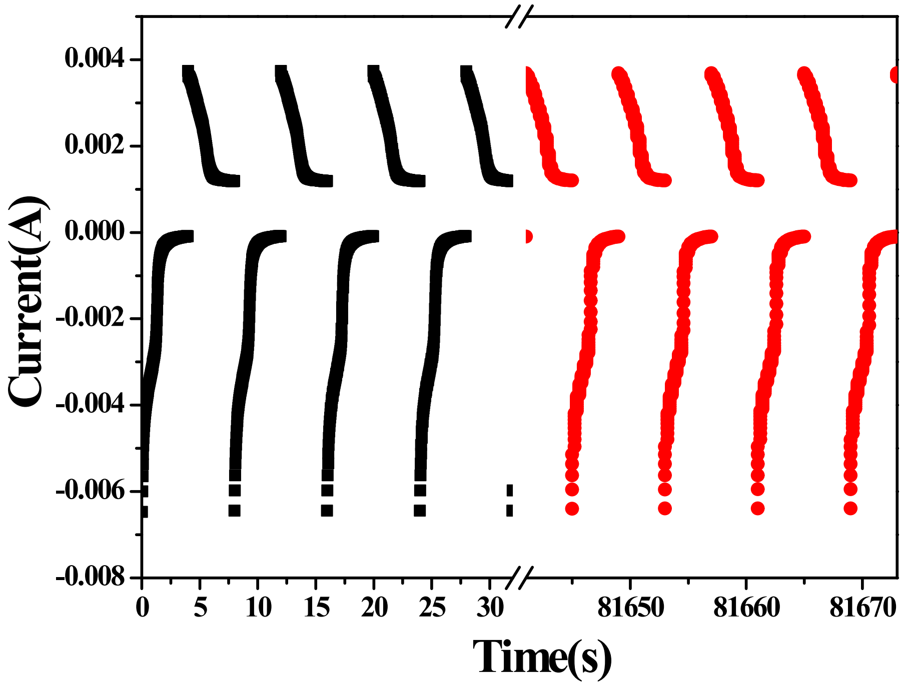

Figure S9 The chronoamperometry curves of the ITO-NiO-2 at 650 nm corresponding to Figure 4 (c)

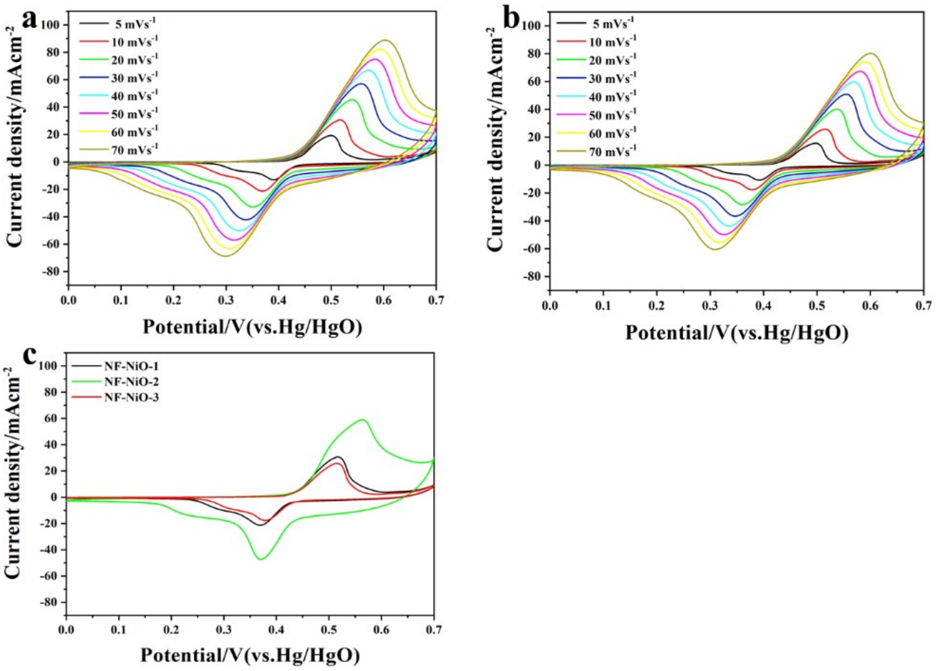

Figure S10. CV curves of NiO film on nickel foam: (a) NF-NiO-1, (b) NF-NiO-3, and (c) CV curves of NF-NiO-1, NF-NiO-2, and NF-NiO-3 at 10 mV s^{-1}.

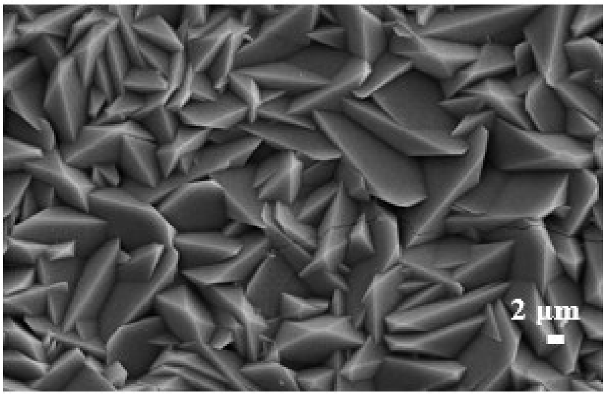

Figure S11. SEM images of Fe_2O_3 film.

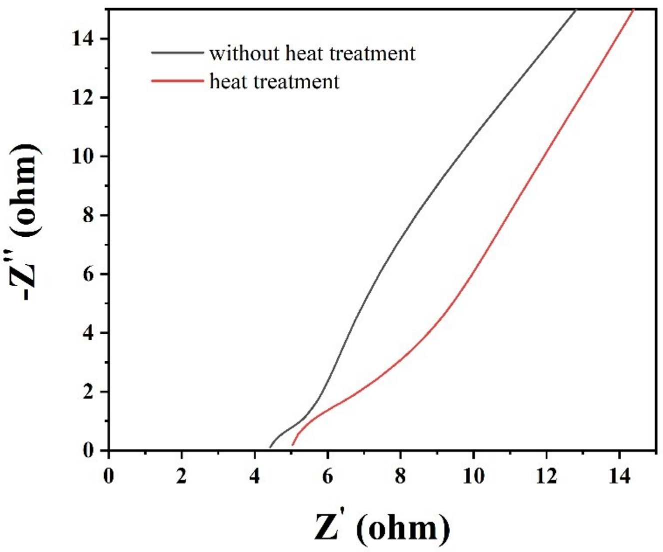

Figure S12. Nyquist plots of the ITO before and after calcinated at 400 ℃ for 2 h.

Two curves have no big differences. It demonstrates that the thermal treatment has no significant influence on the ITO.

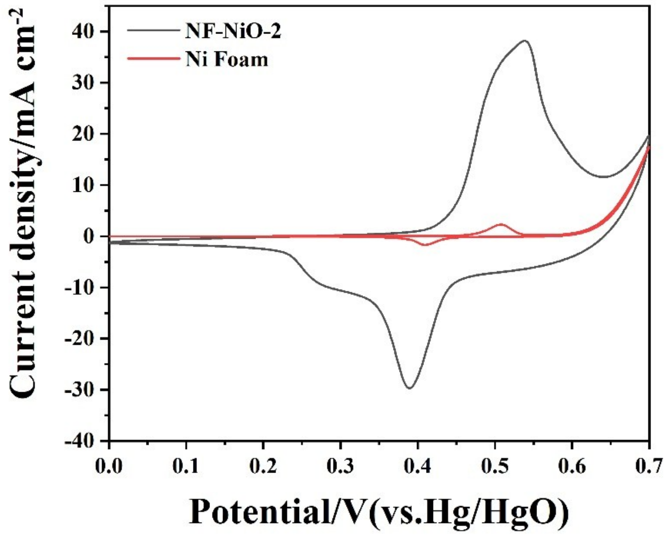

Figure S13. CV curves of NF-NiO-2 and Ni Foam in 1 M KOH at the scan rate of 5 mV s^{-1}.

According to the CV curves of NF-NiO-2 and Ni Foam, the area of CV curve of NF-NiO-2 is much larger than Ni Foam and the contribution to the measured capacity can be neglected.

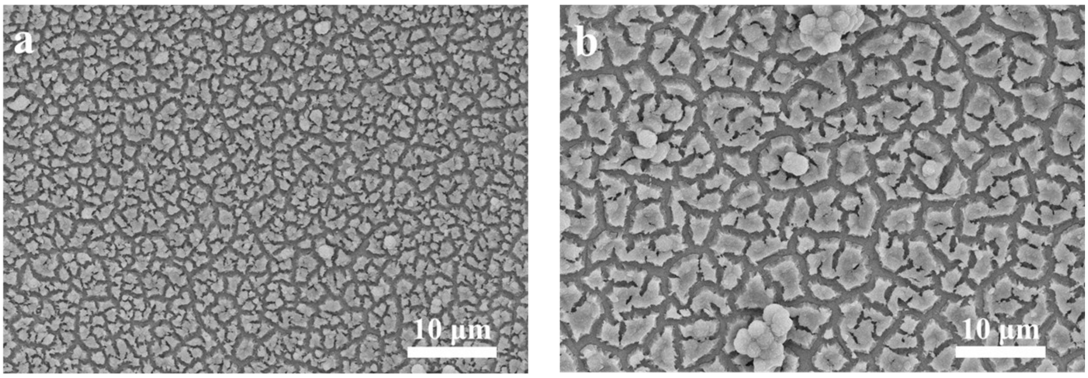

Figure S14. SEM images of NF-NiO-2: (a) before cycling, and (b) after cycling.

It can be seen that the morphology of ITO-NiO-2 maintained well after cycling test, implying good cycling stability.

Table 1 Comparison of the partial properties between NiO in this work and before

Type of materials	Pore distribution	Surface areas	Cycle numbers	References
hierarchical porous NiO	narrow(3-5 nm)	227.5 m^2 g^{-1}	10000	This work
$CoSe_2$@C	broad(5-190 nm)	182.8 m^2 g^{-1}	1000	1
$Ni_{0.65}Co_{0.35}O_2$	broad (1-10 nm)	299 m^2 g^{-1}	5000	2
NiO@C	broad (10-60 nm)	69.7 m^2 g^{-1}	10000	3
$NiCo_2O_4$	broad (8.8-20 nm)	28.5 m^2 g^{-1}	500	4
Ni_2P/Ni	broad (5.2-20 nm)	32.2 m^2 g^{-1}	1000	5
NiO	broad (1.5-20 nm)	69.2 m^2 g^{-1}	10000	6
$CoMoO_4$/Co_3O_4	broad (3.2-60 nm)	59.05 m^2 g^{-1}	2000	7
NiO	broad (1.9-8 nm)	167 m^2 g^{-1}	1600	8
G-NiO@C	broad (3.6-9 nm)	508 m^2 g^{-1}	1000	9

[1] H. Hu, J. L. Liu, H. W. Huang, C. A. Etogo, X. F. Yang, B. Y. Guan, L Zhang, *J. Am. Chem. Soc* **2019**, *141*, 14764.

[2] C. Qu, B. T. Zhao, Y. Jiao, D. C. Chen, S. G. Dai, B. M. Deglee, Y. Chen, K. S. Walton, R. Q. Zou, M. L. Liu, *ACS Energy Lett.* **2017**, *2*, 1263.

[3] H. Liang, R. Li, C. Li, C. Y. Hou, Y. G. Li, Q. H. Zhang, H. Z. Wang, *Mater. Horizons* **2019,** *6*, 571.

[4] H. Li, M. Liang, W. W. Sun, Y. Wang, *Adv. Funct. Mater.* **2016,** *26*, 1098.

[5] X. B. Liu, W. X. Li, X. D. Zhao, Y. C. Liu, W. N. Ce, Z. F. Li, *Adv. Funct. Mater.* **2019**, 1901510.

[6] S. R. Chen, M. Xue, Y. Q. Li, Y. Pan, L. K. Zhua. S. L. Qiu, *J. Mater. Chem. A* **2015**, *3*, 20145.

[7] M. Zhou, F. Lu, X. S. Shen, W. W. Xia, H. Hea, X. H. Zeng, *J. Mater. Chem. A* **2015**, *3*, 21201.

[8] S. K. Meher, P. Justin, G. R. Rao, ACS Appl. Mater. Interfaces **2011**, *3*, 2063.

[9] F. Chen, W. J. Zhou, H. F. Yao, P. Fan, J. T. Yang, Z. D. Fei, M. Q. Zhong, *Green Chem.* **2013**, *15*, 3057.